Hindawi
Advances in Condensed Matter Physics
Volume 2019, Article ID 2710396, 6 pages
https://doi.org/10.1155/2019/2710396

Research Article

Effect of Adding Co on Crystallization Behavior and Magnetoimpedance Effect of Amorphous/Nanocrystalline FeCuNbSiB Alloy Strips

Da-guo Jiang,[1] Yuan-xiu Ye,[1] and Bin Guo[2]

[1]*College of Mathematics and Physics, Jinggangshan University, Jinan 343009, China*
[2]*Network Information Center, Jinggangshan University, Ji'an 343009, China*

Correspondence should be addressed to Bin Guo; 105120398@qq.com

Received 19 November 2018; Accepted 6 January 2019; Published 3 February 2019

Guest Editor: Jun-Cheng Zhang

After one of the B atoms in $Fe_{73.5}Cu_1Nb_3Si_{13.5}B_9$ alloy was replaced by both 0.7 Si and 0.3 Co, $Fe_{73.5}Co_{0.3}Cu_1Nb_3Si_{14.2}B_8$ alloy ribbons were prepared by single roll fast quenching method. The obtained alloy ribbons were subsequently wound into ring magnetic cores, and then these magnetic cores were annealed at different temperatures in air. The effects of adding Co on the crystallization behavior and soft magnetic properties of the as-quenched alloy ribbons with and without heat treatment were studied. The results show that the amorphous structure of the prepared $Fe_{73.5}Co_{0.3}Cu_1Nb_3Si_{14.2}B_8$ alloy ribbons is transformed into the coexistence of amorphous and nanocrystalline structures after heat treatment at 550°C. Comparing with $Fe_{73.5}Cu_1Nb_3Si_{13.5}B_9$ alloy ribbons, the first initial crystallization temperature (T_{x1}) and crystallization peak temperature (T_{p1}) of $Fe_{73.5}Co_{0.3}Cu_1Nb_3Si_{14.2}B_8$ alloy ribbons were reduced by 1.6 and 1.7°C, respectively, While the second initial crystallization temperature (T_{x1}) and crystallization peak temperature (T_{p2}) were increased by 6.5 and 5.7°C, respectively, resulting in that the difference between the first and the second initial crystallization temperatures (ΔT_x) are increased by 8.1°C; the initial permeability (μ_i) and saturation induction density (B_s) of the amorphous/nanocrystalline $Fe_{73.5}Co_{0.3}Cu_1Nb_3Si_{14.2}B_8$ magnetic cores were reduced by 0.15 H/m and 0.39 T, respectively, while the coercivity (H_c) is increased by 0.34 A/m.

1. Introduction

Since a fast quenching process was employed to prepare the amorphous alloys by Klement et al. in 1960 [1], it has been attracting more and more attention of researchers because of its unique structure, efficient preparation process, excellent material properties, and wide application prospects [2]. The amorphous soft magnetic alloy is mainly composed of Fe, Co, and Ni belonging to ferromagnetic metal elements, as well as Si, B, P, and C belonging to amorphous metal elements. Generally, a small amount of transitional elements or rare-earth elements is usually added into the amorphous soft magnetic alloy [3, 4], to improve the ability and thermal stability of the amorphous alloy. Yashizawa et al. found that the iron-based alloy with an amorphous and nanocrystalline dual-phase structure can be conveniently obtained by adding a small amount of Cu and M (M=Nb, Ta, Mo and W, etc.) into the amorphous Fe-Si-B alloy family and annealing them at an appropriate temperature [5].

Panina and Mohrifirstly noticed the giant magnetoimpedance (GMI) effect in the amorphous CoFeSiB soft magnetic alloy wire in 1994, where the impedance value changes with the applied magnetic field along the axis of the wire when the amorphous wire is excited by alternating current [6]. Afterwards, the GMI were also observed in Fe-based nanocrystalline ribbons, films, and wires with high permeability [7, 8]. The various miniature sensors based on GMI have been applied in measurement of weak magnetic fields, detection of azimuth, and magnetic recording technology due to the advantages of this effect such as high sensitivity, small size, and fast response [9].

Both the high temperature properties and high frequency performance of the alloys can be improved by replacing Fe in finemet soft magnetic alloy with Co [10–12]. In this work,

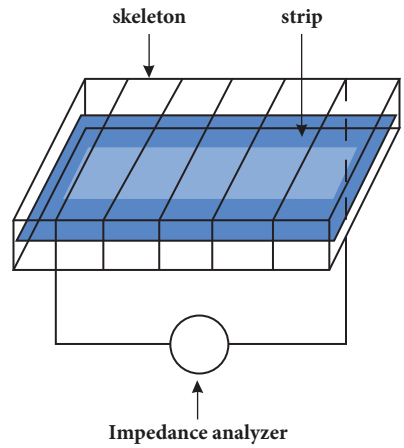

Figure 1: Scheme of testing principle of magnetoimpedance effect.

the $Fe_{73.5}Co_{0.3}Cu_1Nb_3Si_{14.2}B_8$ (Alloy-II (Co)) alloy strip is successfully prepared by signal roll quenching method by adjusting the composition of $Fe_{73.5}Cu_1Nb_3Si_{13.5}B_9$ (Alloy-I). The annealing of the alloy strip at different temperatures is conducted to study the effect of adding Co on the crystallization behavior of the alloy strip. The direct-current (DC) soft magnetic properties of the amorphous/nanocrystalline cores, as well as the magnetic impedance effect of the amorphous/nanocrystalline strips, are also investigated.

2. Sample Preparation and Test Method

The signal roll quenching is employed to prepare the alloy strip of Alloy-I and Alloy-II (Co) with the width 20 mm and thickness 25 μm, respectively. Firstly, the alloy strip is wound into a ring core with an outer diameter of 40 mm and inner diameter of 25 mm by a tape winding machine. Then the end of the strip is welded with amorphous spot welder. Afterwards, the ring core is annealed in a nonmagnetic stainless steel tubular atmosphere resistance furnace in nitrogen atmosphere at the temperature of 350, 400, 450, 500, and 550°C, respectively, and, at each temperature, the duration is 100 min. Finally, the annealed strip is air cooled.

The X-ray diffractometer (XRD) Bruker D-9 is employed to conduct phase analysis. In detail, the copper target K_α rays with wavelength of 0.154 nm, diffraction angle 2θ range of 20~90°, and step size of 0.02° is utilized. The working current and voltage are 40 kV and 40 mA, respectively. The differential thermal analysis is carried on with synchronous thermal analyzer SDT Q600 instrument (TA, America), and the heating rate is $10^\circ C \cdot min^{-1}$. The Argon atmosphere with purity of 99.99% is put to use for protection. Besides, the soft magnetic DC testerMATS-2010SD is employed to test the DC soft magnetic performance. During the process, the amorphous/nanocrystalline cores annealed at 550°C are loaded into the tray in the first place, and then 10 turns of primary coil and 3-turn secondary coil are wound on the guard plate with enameled wires. The effective magnetic path length of amorphous/nanocrystalline cores is 98.44 mm and the effective cross-sectional area is 127.3 mm^2. In addition, the impedance meter 4284A is employed to test the impedance of amorphous/nanocrystalline, and the current amplitude and alternating current frequency are set as 10 mA and 0.1~1 MHz, respectively. The magnetic field drawing instrument is employed to generate magnetic field and the intensity is 0~2800 A/m. Both the DC magnetic field and the current direction are along the length direction of the strip and perpendicular to the geomagnetic field.

As shown in Figure 1, it is the scheme of testing principle of magnetoimpedance effect. The 200-turn copper enameled wire (Φ = 0.21 mm) is layered and evenly wound around the induction coil skeleton (plastic rectangular hollow tube with a section of 7.76 mm in length and 2.15 mm in width and 8.23 mm in length and 3.05 mm in width, respectively). Afterwards, a 2 cm long amorphous/nanocrystalline strip annealed at 550°C is placed in the middle of the inductor skeleton. Finally, the inductor is placed in the center of the magnetic field, and the axial direction of the inductance coil is set to be parallel to the magnetic field.

The effect of impedance is defined as amplitude of impedance variation like

$$\Delta Z = \left| Z_H - Z_0 \right|, \tag{1}$$

where Z_0 is impedance of inductance coil without magnetic field and Z_H is impedance of inductance coil after axial magnetic field applied.

In Figure 2, the equivalent circuit model is displayed to reveal the magnetoimpedance effect. The impedance of alloy strip can be equivalent to the series circuit model of resistance R and inductance L, and the impedance is

$$Z = \sqrt{R^2 + (2\pi f L)^2}, \tag{2}$$

$$L = \frac{\mu N^2 S}{l}, \tag{3}$$

where, in (2), f is the frequency for testing and R and L are the resistance and inductance of the coil, respectively. In (3), N and l stand for the round and length (which is equal to the length of amorphous/nanocrystalline strip) of the coil,

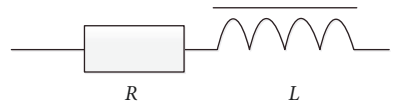

Figure 2: The equivalent circuit model of magnetoimpedance effect.

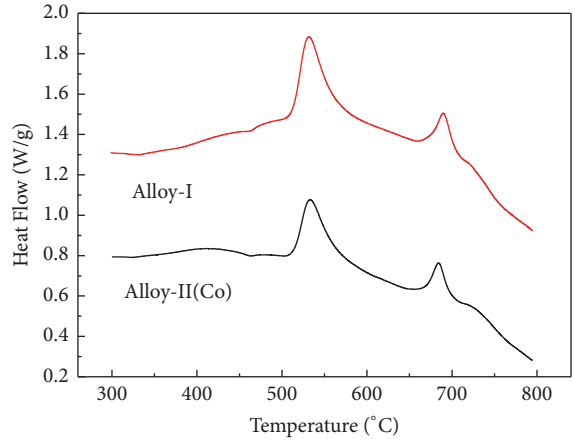

Figure 3: DSC curves of as-quenched alloy strips.

respectively. μ and S represent the magnetic permeability of the amorphous/nanocrystalline strip and cross section area of coil, respectively.

From (1), (2), and (3), the impedance of amorphous/nanocrystalline strip can be calculated by

$$\Delta Z = |Z_H - Z_0| = \left| \sqrt{R^2 + \left(\frac{2\pi f \mu_h N^2 S}{l}\right)^2} - \sqrt{R^2 + \left(\frac{2\pi f \mu_0 N^2 S}{l}\right)^2} \right|, \quad (4)$$

where μ_0 is the permeability of amorphous/nanocrystalline strip without magnetic field, while μ_h denotes the permeability of amorphous/nanocrystalline strip after axial magnetic field is applied.

3. Result and Analysis

3.1. Effect of Adding Co on Amorphous and Crystallization Behavior of Alloy Strip. As can be seen from Figure 3, both quenched alloy strips have a two-stage crystallization process. In the first stage, the starting crystallization temperatures are 514.4 and 512.8°C, respectively, while the crystallization peak temperatures are 533.4 and 531.7°C, respectively. Regarding the second stage, the starting crystallization temperatures are 665.4 and 671.9°C, respectively, and the crystallization peak temperatures are 684.1 and 689.8°C, respectively. The differences of the starting crystallization temperature of the two stages are 151 and 159.1°C, respectively.

As shown in Figure 4, the diffraction spectra of two kinds of alloy strip with different quenched states perform typical diffuse peak characteristics of amorphous structure, and there are no sharp diffraction peaks in the crystalline phase. It indicates that both of the alloy strips with different quenched states possess noncrystalline structure. The strength of the diffuse peaks of the two alloy strips increases but the diffuse peak width is gradually narrowed at 2θ of=45° along with the increasing of annealing temperature. When the annealing temperature reaches 500°C, the sharp diffraction peaks appear at 2θ with=44.7°, 65°, and 82° for the both alloy strips. With comparison to the PDF card (35-0519), the crystal surfaces including (110), (200), and (211) belonging to the Fe_3Si phase with body centered cubic (BCC) structure can be clearly identified. On the other hand, when the annealing temperature comes to 550°C, the diffraction peak intensity of Alloy-II (Co) alloy strip gets stronger, and the width of the peak is narrower compared to Alloy-I alloy strip. Judged from Scherrer equation, the grain sizes of Alloy-I and Alloy-II (Co) alloy strips can be calculated to be about 11.044 and 12.734 nm at 2θ of =44.7°, respectively. It reveals that both alloy strips can form a composite structure with the coexistence of the amorphous and nanocrystalline phases superior to heat treatment at 550°C.

From the results in Figures 3 and 4, we find that the first crystallization peak corresponds to the precipitation of soft magnetic solid solution (precipitation of α-Fe phase). And the second crystallization peak is the crystallization of the remaining amorphous phase, which is mainly related to the precipitation of Co-B, Fe-B, and Nb-Co compounds [13–15]. Compared to the Alloy-I alloy strip, the Alloy-II (Co) one possesses lower starting crystallization temperature and crystallization peak temperature, which indicates that the Co addition will lead to worse thermal stability of amorphous alloy [16, 17]. However, the addition of Co increases the difference between the one- and two-stage crystallization temperature of the alloy strip, which is conducive to the precipitation of a single Fe-Si phase and the precipitation of

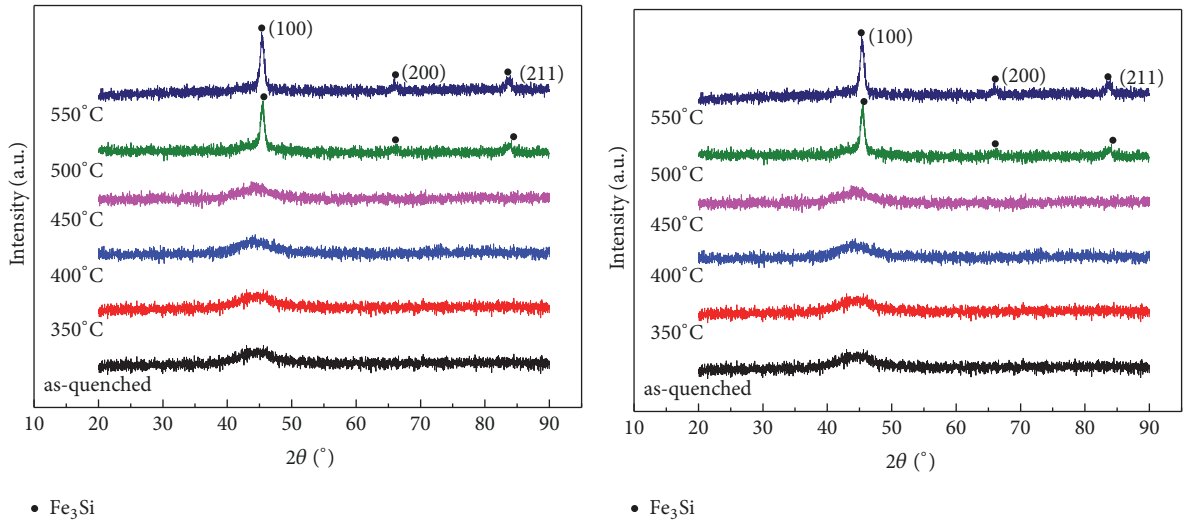

(a) Alloy-I alloy strips

(b) Alloy-II (Co) alloy strips

Figure 4: XRD patterns of as-quenched and annealing alloy strips.

Fe-B phase which affects the magnetic properties of the alloy. Actually, Co element possesses similar chemical property to Fe, and if Co element is added to the amorphous alloy system, solid solution will be formed. In this process, Co atoms increase the chaos of the alloy melt by occupying the spatial lattice position of the Fe atoms, resulting in formation of amorphous phase. Besides, the addition of Co element can delay the occurrence of crystallization reaction and restrict the precipitation of amorphous phase, which also promotes the formation of amorphous phase.

3.2. Effect of Adding Co on DC Soft Magnetic Properties of Amorphous/Nanocrystalline Crystalline Cores. The effect of adding Co on DC soft magnetic properties of amorphous/nanocrystalline cores is displayed in Table 1, where μ_i and μ_m mark the initial and maximum permeability, respectively; B_s and B_r represent the saturation magnetic induction intensity and residual magnetism, respectively. The hysteresis loss and coercive force are denoted by P_u and H_c, respectively. Compared with the amorphous/nanocrystalline Alloy-I core, the amorphous/nanocrystalline Alloy-II (Co) magnetic cores possesses lower initial permeability, maximum magnetic permeability, hysteresis loss, saturation magnetic induction, and residual magnetism, but it yields to coercive force. This trend shows that adding Co element reduces the DC soft magnetic properties of amorphous/nanocrystalline cores. The decrease of initial permeability can improve the antisaturation ability and antibiasing ability of amorphous/nanocrystalline magnetic core under DC bias, to some extent. In particular, the stability of the amorphous/nanocrystalline core can be greatly improved in the electromagnetic application environment with DC component.

3.3. Effect of Adding Co on Magnetic Impedance of FeCuNbSiB Amorphous/Nanocrystalline Strip. The magnetoimpedance effect of the amorphous/nanocrystalline Alloy-I strip annealed at 550°C is shown in Figure 5. The results indicate that the impedance Z and amplitude of the impedance ΔZ increase as the test frequency f increases when the magnetic field strength H is fixed at constant. On the other side, when the test frequency f remains unchanged, the impedance Z will decrease but the amplitude of the impedance ΔZ is just the opposite along with the increase of H which is the magnetic field strength. In fact, given a coil with resistance R, number of turns N, cross section area S, and length l, the permeability μ of amorphous/nanocrystalline strip is constant if the magnetic field intensity H remains unchanged, leading to increase of impedance Zas the increase of test frequency f from (2) and (3). However, the permeability μ of the amorphous/nanocrystalline strip decreases with the increase of magnetic field intensity H when the test frequency f is constant [8], following decrease of the impedance Z as the increase of magnetic field strength H according to (2) and (3).

In addition to the above discussion, Z_H will decrease along with the increase of magnetic strength H since Z_0 is a constant if the test frequency f remains to be unchanged, resulting in the increase of ΔZ as the increase of H according to (4), while μ_H is constant if the magnetic strength H stays in the same condition, with the increase of ΔZ as increase of f from (4).

In Figure 6, the magnetoimpedance effect of the amorphous/nanocrystalline Alloy-I and Alloy-II (Co) strips annealed at 550°C is tested and shown, where the test frequency is 1.0MHz. The results show that the impedance variation amplitude ΔZ of the amorphous/nanocrystalline Alloy-II (Co) strip increases compared to the Alloy-Ione.

4. Conclusion

In conclusion, the following two aspects can be attributed in this work:

(1). The amorphous $Fe_{73.5}Co_{0.3}Cu_1Nb_3Si_{14.2}B_8$ strip is successfully prepared by single roll quenching method by

Table 1: DC soft magnetic properties of the amorphous/nanocrystalline cores heat treatment at 550°C.

Magnetic core	μ_i/(H·m^{-1})	μ_m/(H·m^{-1})	P_u/(T·A·m^{-1})	B_s/T	B_r/T	H_c/(A·m^{-1})
Alloy-I	0.39	0.99	2.77	1.52	0.76	0.40
Alloy-II (Co)	0.24	0.61	1.9	1.13	0.64	0.74

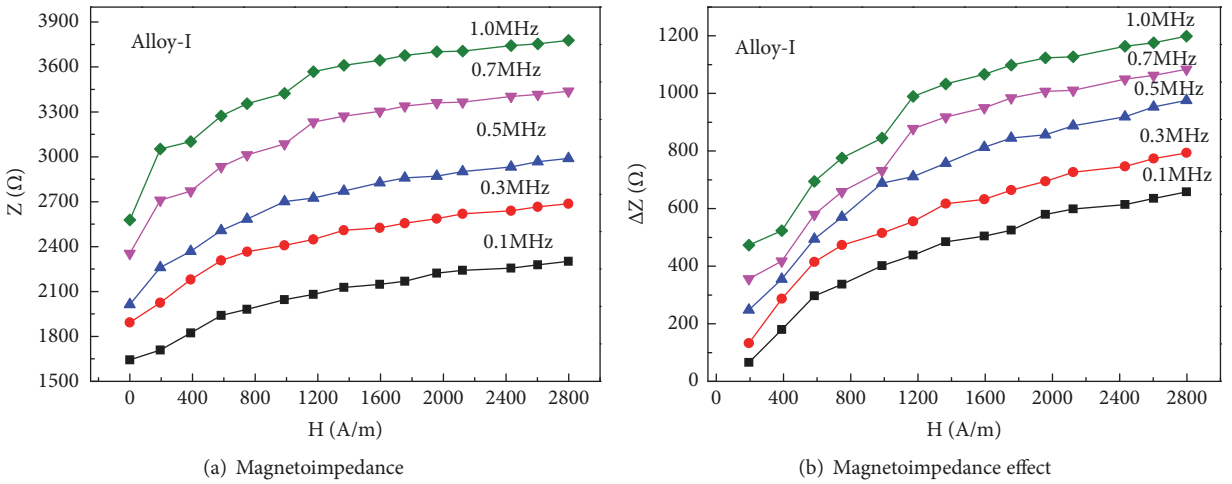

Figure 5: The magneto impedance effect of the Alloy-I amorphous/nanocrystalline strips after heat treatment at 550°C.

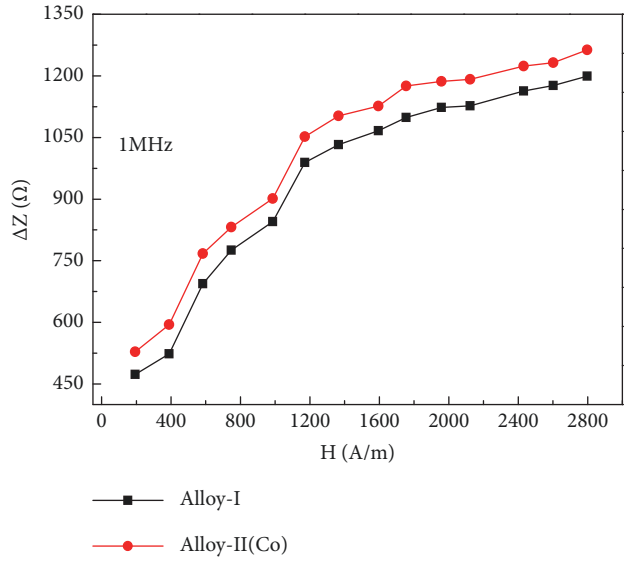

Figure 6: The magnetoimpedance effect of Alloy-I and Alloy-II(Co) amorphous/nanocrystalline strips after heat treatment at 550°C.

replacing one B atom with 0.7 Si and 0.3 Co based on the $Fe_{73.5}Cu_1Nb_3Si_{13.5}B_9$ alloy. Both amorphous strips can be formed, the amorphous/nanocrystals dual-phase structure after heat treatment at 550°C. Compared to the amorphous $Fe_{73.5}Cu_1Nb_3Si_{13.5}B_9$ strip, both the first-stage initial crystallization temperature and crystallization peak temperature of the amorphous $Fe_{73.5}Co_{0.3}Cu_1Nb_3Si_{14.2}B_8$ ribbon get lower, but both the initial crystallization temperature and the crystallization peak temperature are higher in the second stage, and the difference of initial crystallization temperatures increases between the two stages.

(2). The initial magnetic permeability, saturation magnetic induction, and the DC soft magnetic properties of the amorphous/nanocrystalline $Fe_{73.5}Co_{0.3}Cu_1Nb_3Si_{14.2}B_8$ magnetic core are all reduced, but it yields to the coercive force compared with the amorphous/nanocrystalline $Fe_{73.5}Cu_1Nb_3Si_{13.5}B_9$ magnetic core. In addition, the impedance amplitude of the amorphous/nanocrystalline

$Fe_{73.5}Co_{0.3}Cu_1Nb_3Si_{14.2}B_8$ strip increases compared to the amorphous/nanocrystalline $Fe_{73.5}Cu_1Nb_3Si_{13.5}B_9$ strip.

Data Availability

The data used to support the findings of this study are included within the article. And the shared data allows both the Hindawi publisher and other researchers to verify the results of an article, replicate the analysis, and conduct secondary analyses.

Conflicts of Interest

The authors declare that they have no conflicts of interest.

References

[1] W. Klement, R. H. Willens, and P. Duwez, "Non-crystalline structure in solidified Gold-Silicon alloys," *Nature*, vol. 187, no. 31, pp. 869-870, 1960.

[2] R. Hasegawa, "Applications of amorphous magnetic alloys in electronic devices," *Journal of Non-Crystalline Solids*, vol. 287, no. 1/2/3, pp. 405–412, 2001.

[3] J. Daguo, Y. Yuanxiu, and Y. Caobing, "Magnetic induction effect of rare-earth La modified $Fe_{78}Si_9B_{13}$ amorphous ribbons," *Material for Mechanical Engineering*, vol. 38, no. 3, pp. 66–69, 2014.

[4] G. Bin, Y. Yuanxiu, J. Daguo, A. Hui, and W. Zhihui, "Glass forming ability and magneto impedance effect of FeCuNbSiB-La alloy strips," *Ordnance Material Science and Engineering*, vol. 38, no. 4, pp. 22–25, 2015.

[5] Y. Yoshizawa, S. Oguma, and K. Yamauchi, "New Fe-based soft magnetic alloys composed of ultrafine grain structure," *Journal of Applied Physics*, vol. 64, no. 10, pp. 6044–6046, 1988.

[6] K. Mohri, T. Kohzawa, k. Kawashima et al., "Magnetor induced effect in amorphous wires," *IEEE Trans Magn*, vol. 28, no. 2, pp. 3150–3152, 1992.

[7] H. Qin, J. Hu, B. Li, and R. Zhang, "Giant magnetoimpedance effect in Fe-Cu-Nb-Si-B as-cast ribbons," *Rare Metal Materials and Engineering*, vol. 35, no. 2, pp. 270–272, 2006.

[8] J. Daguo, F. Yuan, Z. Zhenghou, S. Hui et al., "Magneto impedance effect of FeSiB amorphous alloy ribbons," *Hot Working Technology*, vol. 39, no. 10, pp. 37–39, 2010.

[9] J. Daguo, Z. Zhenghou, S. Hui et al., "Influence factors of Magnet-inductive effect of $Fe_{73.5}Cu_1Nb_3Si_{13.5}B_9$ amorphous alloy ribbons," *Materials for Mechanical Engineering*, vol. 33, no. 4, pp. 29–34, 2009.

[10] B. K. Aleksandra, K. Roman, K. Tadeusz et al., "Magnetic properties of Co doped finemet at elevated temperature," *Reviews on Advanced Materials Science*, vol. 18, no. 6, pp. 545–548, 2008.

[11] M. Danning, Y. Changlin, and W. Xiaowei, "Research development of FeCoalloy soft magnetic materials," *Rare Metal Materials and Engineering*, vol. 42, no. 6, pp. 1316–1319, 2013.

[12] L. Liya, Y. Jianghong, G. Yicheng et al., "Nanocrystallization and microstructure of $(FeCo)_{73.5}Cu_1Nb_3Si_{13.5}B_9$," *Journal of Central South University (Science and Technology)*, vol. 39, no. 3, pp. 522–526, 2008.

[13] D. Yanhong, *Investigation on Magnetic Properties of Nanocrystalline Fe-Co-Cu-Nb-Si-B Soft Magnetic Alloys [M. S. thesis]*, Tianjin University of Technology (Tian Jin), 2004.

[14] M. Xiaohua, W. Zhi, and W. Guangjian, "Microstructures and high-frequency magnetic properties of nanocrystalline $(Fe_{1-x}Co_x)_{78.4}Nb_{2.6}Si_9B_9Cu_l$ soft magnetic alloys," *ActaMetallurgicaSinica*, vol. 43, no. 3, pp. 281–285, 2007.

[15] D. Yanhong, L. Mingji, Y. Baohe et al., "AC magnetic properties of $Fe_{15.38}Co_{61.52}Cu_{0.6}Nb_{2.5}Si_{11}B_9$ nanocrystalline soft magnetic alloy," *ActaPhysicaSinica*, vol. 69, no. 9, pp. 0975021–0975025, 2011.

[16] Y. Jia, Z.-J. Wei, M.-Z. Ma, S.-Y. Zeng, and W.-K. Wang, "Thermal stability and crystallization process of FeCoNbSiBCu bulk metallic glasses," *Journal of Materials Engineering*, vol. 36, no. 6, pp. 33–35, 2008.

[17] Y. Wanqiu, L. Dong, S. Yaming et al., "Effect of Co content on thermal stability and microstructure of $Fe_{80-x}Co_xZr_8Mo_2B_9Cu_1$ alloys," *Transactions of Materials and Heat Treatment*, vol. 35, no. 12, pp. 146–149, 2014.